Ref. Ares(2026)6580005 - 30/06/2026

CON CERTO

Deliverable D5.3 – Synthesis report on preliminary developments of hydrology, energy, and nitrogen cycles

Lead Beneficiary: CMCC

Authors: Daniele Peano, Barbara Cardeli, Matteo Mastropierro, Jose Costa Saura, Giulia Mengoli, Manuela Balzarolo, Beata Opacka, Trissevgeni Stavrakou, Jean-Francois Müller, Glenn-Michael Oomen, Souhail Boussetta, Anna Agusti-Panareda, Patricia de Rosnay, Sebastien Garrigues

30/06/2026

Funded by
the European Union

Prepared under contract from the European Commission

Grant agreement No. 101185000

Project acronym:	CONCERTO
Project full title:	Improved CarbOn cycle represeNtation through multi-sCale models and Earth obseRvation for Terrestrial ecOsystems
Start of the project:	January 2025
Duration:	48 months
Project coordinator:	Manuela Balzarolo
Deliverable title:	Synthesis report on preliminary developments of hydrology, energy, and nitrogen cycles
Deliverable n°:	D5.3
Nature of the deliverable:	Report
Dissemination level:	Public
WP responsible:	WP5
Lead beneficiary:	CMCC
Citation:	Peano D., Cardeli B., Mastropierro M., Costa Saura J., Mengoli G., Balzarolo M., Opacka B., Stavrakou T., Müller J.-F., Oomen G.-M., Boussetta S., Agusti-Panareda A., de Rosnay P., Garrigues S. (2026). ***Synthesis report on preliminary developments of hydrology, energy, and nitrogen cycles***. Deliverable D5.3. Horizon Europe CONCERTO project, Grant Agreement No 101185000.
Due date of deliverable:	Month n° 18
Actual submission date:	Month n° 18
Deliverable status:	Submitted

Version	Status	Date	Author(s)/Reviewer
1.0	Draft	05 June 2026	CMCC, BIRA, ECMWF
2.0	Final	30 June 2026	CMCC, BIRA, ECMWF, ICL, UT

Contents

1. Preface

The activities performed within the Working Package 5 (WP5) of the CONCERTO project aim to improve the representation of the main land carbon processes within the land surface models (LSMs), the land component of state-of-the-art Earth system models (ESMs). In particular, WP5 activities leverage data coming from the first and second Working Packages (WP1 and WP2) as novel boundary conditions for LSMs and references for model developments. Besides, the developments achieved in the third and fourth WPs (WP3 and WP4) are complementary to the activities performed in WP5. Finally, WP5 developments provide the basis of the planned simulations of the sixth Working Package (WP6) (Figure 1).

The present deliverable describes the status of developments within the task 2 of WP5, focusing on the development of the LSMs representation of interactions between the carbon cycle and other climate system cycles, i.e. nitrogen and water cycles, and disturbances, such as fire and volatile organic compound emissions.

The outcomes presented in this deliverable are to be considered as preliminary results, since the task results will be obtained in month 36 and summarised in deliverable D5.4. The status of each activity within the task 2 of WP5 is listed in Table 1.

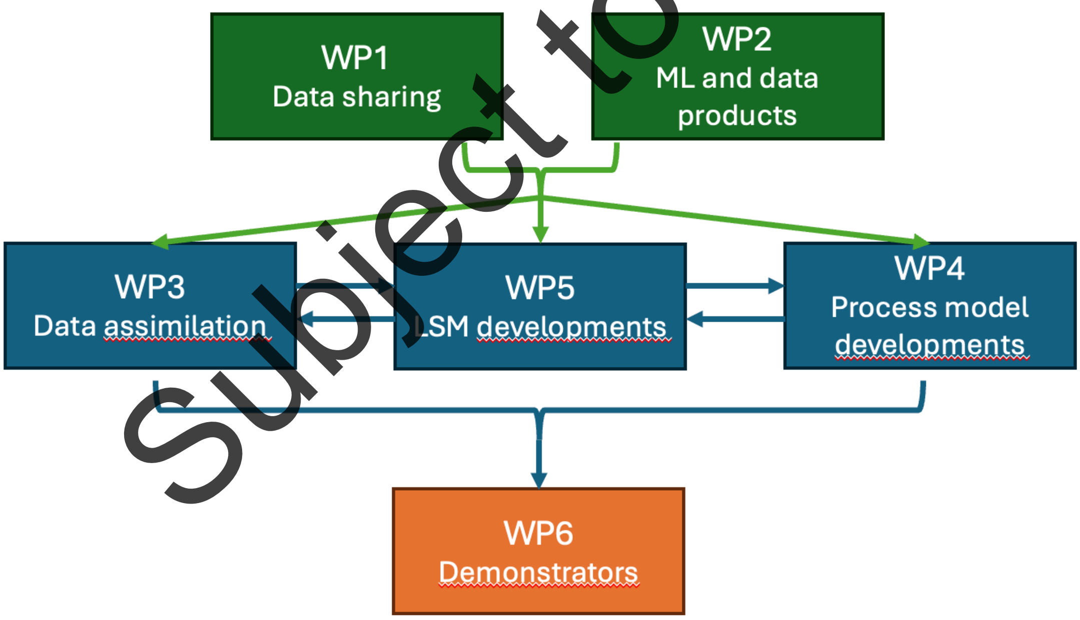

Figure 1: Schematic of CONCERTO work packages in relation to WP5.

Table 1: Summary of the status of development for each activity of the second task of WP5. Complete stands for developments that reached their conclusion; Ongoing stands for developments started within the initial 18 months of the project and will continue in the next 18-month period; Planned stands for developments in their preliminary stages and that will be developed during the next 18 months.

Activity	Status
Freshwater transport of carbon	Planned
Improving nitrogen cycle	Ongoing
Development of the fire module	Ongoing
Improve BVOC module in CLM	Ongoing
Coupling transpiration with plant assimilation	Ongoing

2. Summary

This deliverable provides a brief summary of the ongoing development performed in task 2 of CONCERTO's WP5. The principal aim of these developments is to improve the representation of the inter-connections between the carbon cycle and other climate system cycles, in particular water and nitrogen cycles, disturbances, such as fires, and biogenic volatile organic compound (BVOC) emissions within a set of state-of-the-art LSMs.

The interplay between the carbon and water cycles is implemented in the ecLand LSM by coupling a dynamically varying Leaf Area Index (LAI) scheme with the land physical component and a novel scheme that represents the influence of transpiration on plant assimilation, using the same canopy pathway for both water and carbon. This approach primarily affects areas with low vegetation. Besides that, a river transport scheme coupled to the Community Land Model (CLM) simulates the transport of carbon from land to the ocean coast to close the global carbon budget and link carbon and water cycles. This implementation is at its preliminary stages and will be finalised in the following months and summarised in the companion deliverable, D5.4.

Nitrogen and carbon are key biogeochemical cycles in the climate system, and they are strongly linked. LSMs usually apply stoichiometric relations between nitrogen and carbon to represent the ratio between these two compounds. Consequently, limitations in representing the nitrogen cycle increase the uncertainties in the simulated carbon cycle. In this framework, CONCERTO WP5 improves the representation of nitrification and denitrification in CLM using the "hole-in-the-pipe" approach and including soil pH as a driver of both processes (val Martin et al., 2023). In this approach, the soil nitrogen cycle is conceptualised as a unidirectional flow in which nitrification and denitrification act as successive segments, while lateral "holes" represent the gaseous escape of nitrous oxide (N_2O) and nitric oxide (NO), modulated by environmental drivers such as soil pH. The new approach and the addition of soil pH induce an indirect response in the carbon cycle by modulating the simulated nitrogen use efficiency and foliar stoichiometry.

Moreover, vegetation provides the main source of Biogenic Volatile Organic Compounds (BVOCs, such as isoprene, pentane, hexane, and others), and the representation of carbon stocks in leaves, through the LAI, influences the ability of LSMs to represent the impact of vegetation on ozone formation, atmospheric composition, and atmospheric aerosol concentrations. In WP5, the influence of temperature, vegetation (i.e. LAI), and soil moisture conditions on the simulated emissions of BVOCs is investigated due to large uncertainties in models'

representations of this relationship. In particular, the soil moisture emission factor of the MEGAN module is improved in both CLM and MEGAN-MOHYCAN frameworks. The changes in the MEGAN dry factor improve the ability of both models to simulate the BVOC emissions. However, discrepancies with observations remain, and further investigation will continue within the WP5 activities.

The vegetation amount is the main source of fuel in the fire module implemented within LSMs. Since LSMs are still unable to properly capture the burned area and, consequently, fire carbon emissions, one of the tasks of CONCERTO in WP5 is to improve the representation of fuel variability based on the carbon distribution between vegetation tissues, such as leaves and stems, and litter. In particular, the simulated variability of fuel availability increases when CLM accounts for live and dead fine fuel, i.e. leaves and litter.

3. List of Abbreviations

2D – 2m Dew point temperature

2T – 2m Temperature

BVOC - Biogenic Volatile Organic Compound

CDR – Carbon Dioxide Removal

CLM - Community Land Model

CRF – Canopy Reduction Factor

ERW – Enhanced Rock Weathering

ESM - Earth System Model

IFS – Integrated Forecasting System

LAI - Leaf Area Index

LSM - Land Surface Model

MEGAN - Model of Emissions of Gases and Aerosols from Nature

NUE – Nitrogen Use Efficiency

NWP – Numerical Weather Prediction

RMSE – Root Mean Square Error

SOA - Secondary Organic Aerosols

WP - Working Package

4. Water cycle

4.1. Status of developments

4.1.1. Transpiration and plant assimilation

In order to improve the coupling between water, energy and carbon cycles, two new developments are tested within the ECMWF system. The first is to couple the new prognostic LAI module in ecLand (Boussetta et al., 2021) to the ECMWF Integrated Forecasting System (IFS) allowing the water and carbon fluxes to be better constrained by the vegetation variability at different temporal scales and assess its impact on the coupled surface-atmosphere system. The second is to explicitly couple the plant transpiration with the carbon assimilation by using the same canopy pathway from the Farquhar model for both water and CO_2.

Coupling the prognostic LAI

After coupling the new prognostic LAI (D5.1) to the integrated forecasting system (IFS), forecasts experiment with and without prognostic LAI are run over 2017 at the cubic octahedral reduced Gaussian grid Tco319 with an approximate horizontal grid spacing of 36 km in mid-latitudes. The impact of the prognostic LAI is assessed for the 2m dew point temperature (2D) and the 2m temperature (2T) operational analysis where various satellites and in-situ observations are assimilated (Geer et al., 2016).

Mixed results are seen across seasons, while for June-July-August (JJA) we see an overall moistening and cooling except for the Amazon, East Asia and India, resulting in an overall reduction of the 2T Root Mean Square Error (RMSE) except for the daytime in south Africa and Europe where the 2T scores are degraded (Figures 3). The 2D scores are also degraded over Europe for day and night times but improves elsewhere (Figures 2). In March-April-May (MAM) both 2T and 2D scores improve during day and night over Europe and degrade in Southern Africa (Figures 4 and 5 upper). This impact is related to a slight warming/drying over Europe and a cooling/moistening in southern Africa (Figures 4 and 5 lower). To note that the regions where the 2m observations coverage is low, the scores are mostly related to the operational model.

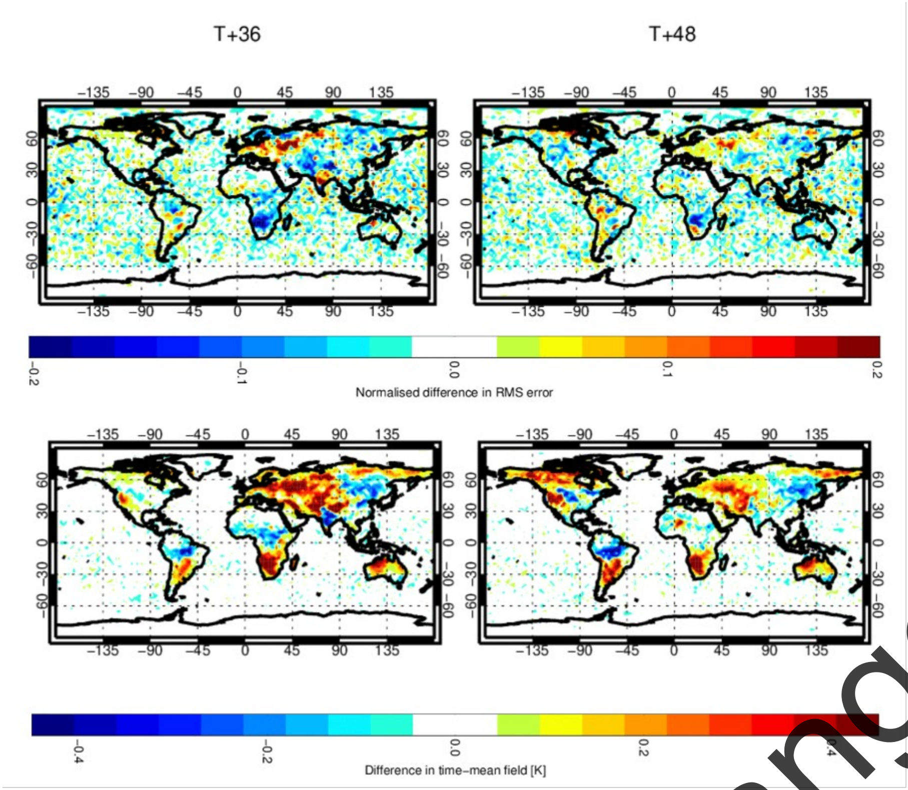

Figure 2: JJA 2D RMSE normalised difference w.r.t the control operational analysis at 36h and 48h lead times where blue colour reflects a reduction of the error (upper); 2D difference from the control experiment where no prognostic LAI coupling is considered at the same lead times where blue colour here reflects a reduction in 2D (lower)

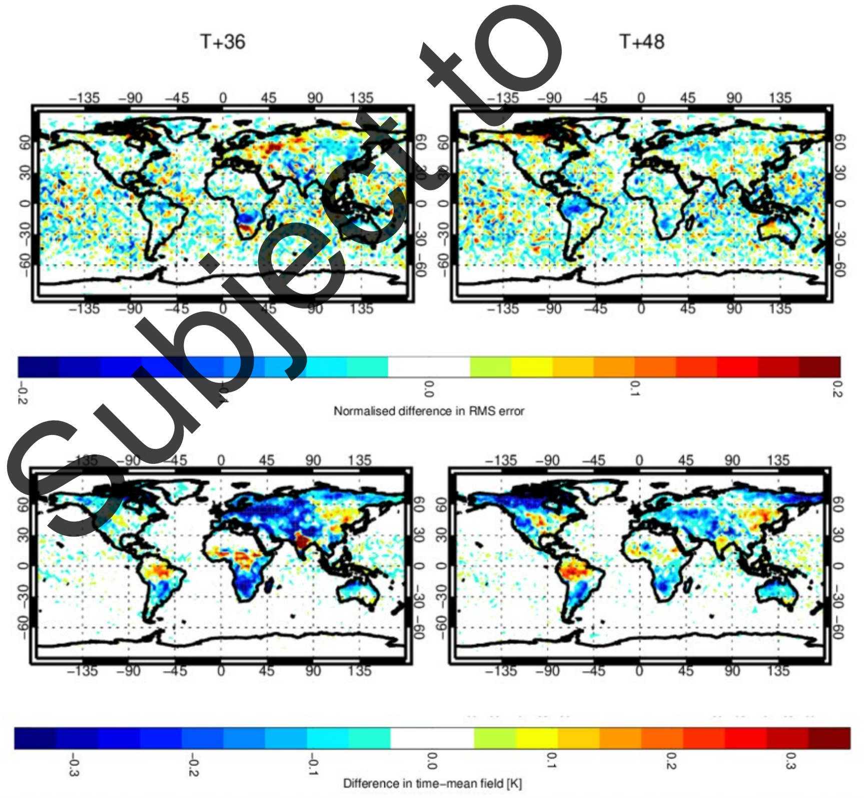

Figure 3: same as Figure 2 for the 2T

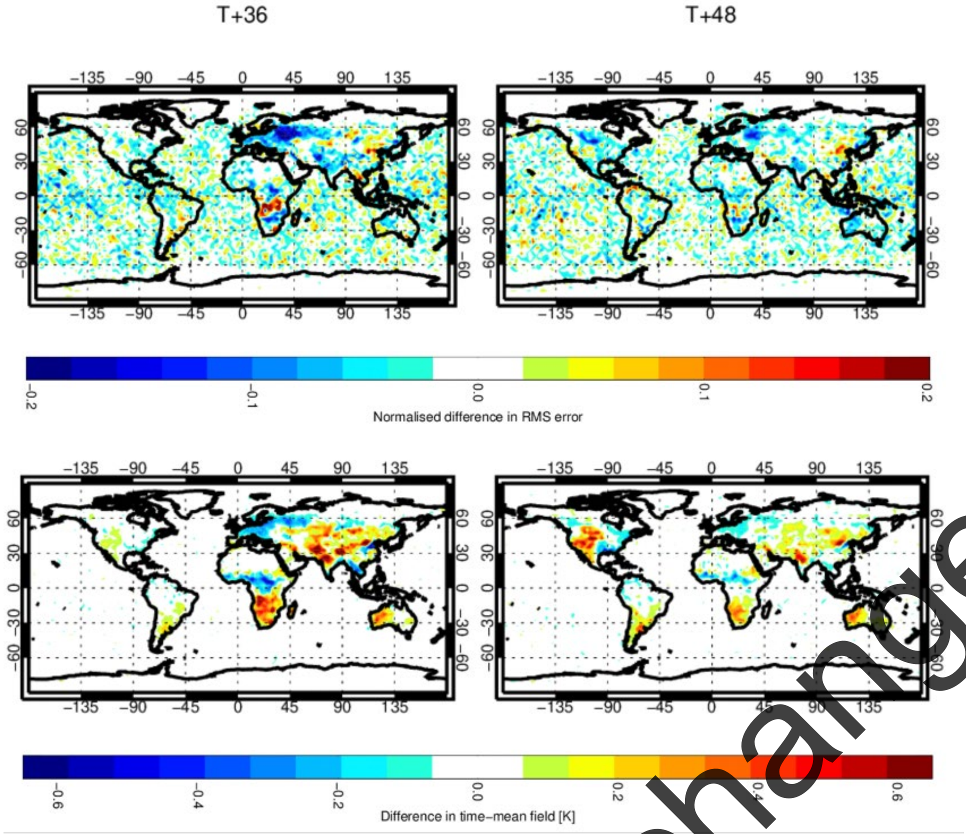

Figure 4: MAM 2D RMSE difference (upper)as compared with the operational analysis, 2D difference from the control experiment where no prognostic LAI coupling is considered (lower)

Coupling the water and Carbon pathways:

The current operational setting in ecLand within the IFS relies on the Jarvis (Jarvis, 1976) parametrisation for the evapotranspiration and the Farquhar (Farquhar et al., 1980) parametrisation for the carbon fluxes. This modular setting was chosen to allow modifications to the carbon parametrisation while preserving evapotranspiration and numerical weather prediction (NWP) scores. Given that CO_2 and water vapor have the same pathway through the plant stomata, in this project we are exploring the use of an "equivalent" canopy resistance extracted the GPP computation in Farquhar for the estimation of the plant evapotranspiration.

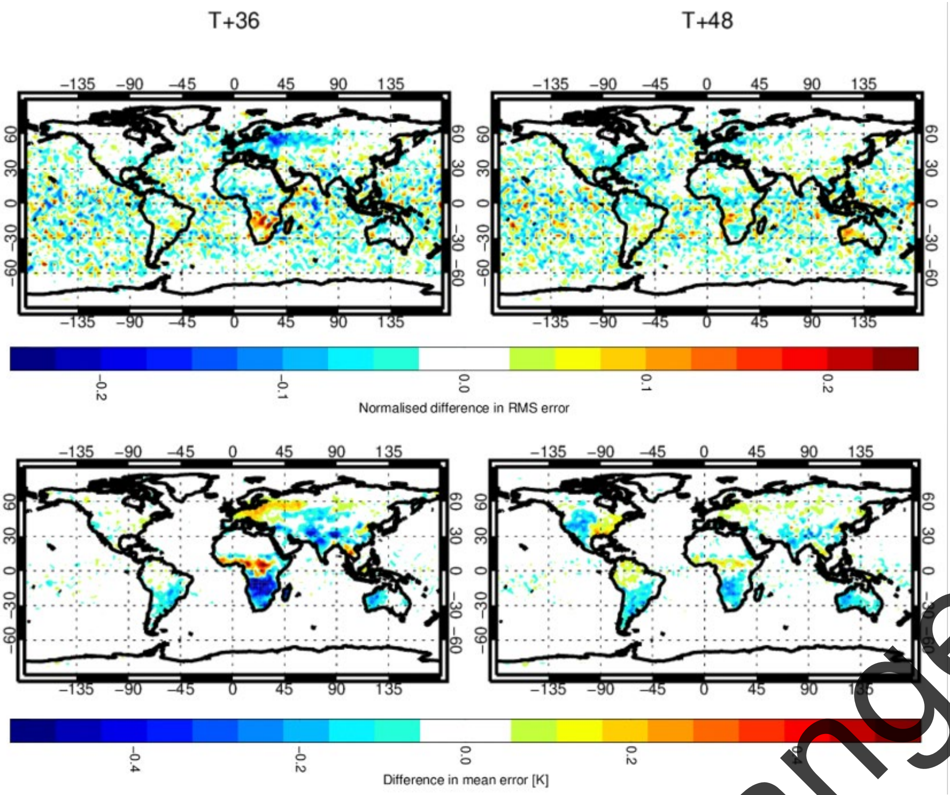

Figure 5: same as Figure 4 for the 2m Temperature

To minimise spin-up issues due to non-balanced initialisation of the surface state, data assimilation experiments with and without coupling the CO_2 flux and the evapotranspiration parametrisations are run for June-July 2022 at Tco399 cubic octahedral reduced Gaussian grid (approximate horizontal grid spacing of 25 km in mid-latitudes). In this case, an initial assessment is done for the upper air temperature and relative humidity at 850hpa. Using the same canopy resistance for CO_2 flux and evapotranspiration resulted in a reduction of the 850hpa relative humidity and increase in the air temperature (Figure 6). These changes have mixed impact on NWP scores. While relative humidity RMSE is strongly improved over northern hemisphere forests, it is degraded in the tropic (Figure 7 upper). An improvement is also seen in the air temperature; however, temperature scores' degradation is extended to areas with dominance of low vegetation like crop area in India and East US or crops and grass in central Europe (Figure 7 lower).

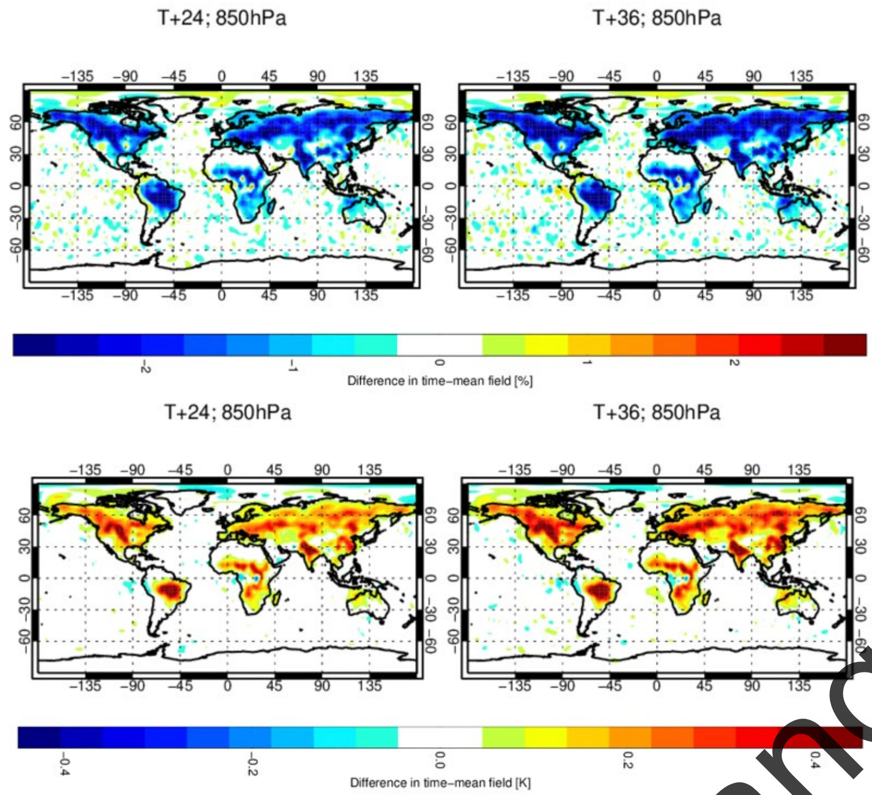

Figure 6: Differences between the case of coupled CO2 flux with evapotranspiration and the uncoupled case where CO2 flux and evapotranspiration are computed Independently; for Relative humidity at 850hpa (upper) and air temperature at 850hpa (lower)

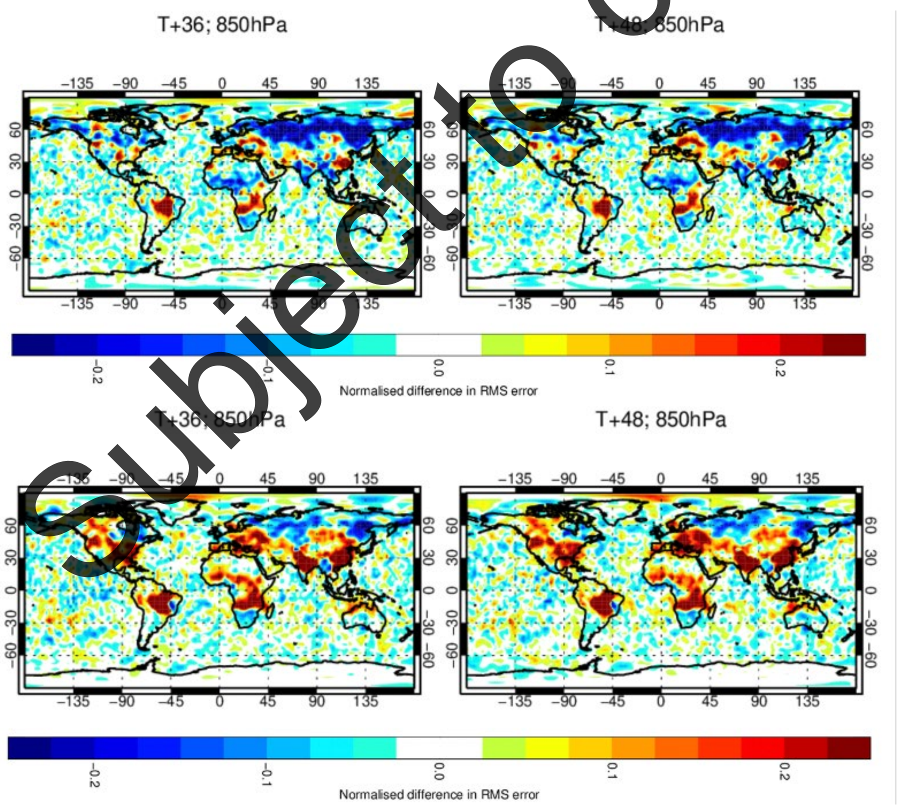

Figure 7: Same as Figure 4 for the RMSE w.r.t operational analysis. For the relative humidity at 850hPa (upper), and the air temperature at 850hPa (lower).

4.2 Future developments

4.2.1. Freshwater transport of carbon

Rivers connect land and ocean biogeochemistry (da Cunha et al., 2007). The amount of carbon and nutrients in coastal areas plays a crucial role in determining whether marine and oceanic ecosystems work as CO_2 sinks or sources, in turn impacting the global carbon budget (Smith and Hollibaugh, 1993). Consequently, the transport of carbon and nutrients (e.g. nitrogen) will be implemented in the river routing scheme coupled with CLM, exploring an improved CLM's configuration that refines NO fluxes and the NH_3 volatilisation.

4.2.2. Transpiration and plant assimilation

The coupling of the carbon and water cycle in ecLand is now achieved with two distinct options, the first through the coupling of the prognostic LAI module with the IFS allowing changes in the carbon cycle to also affect the evapotranspiration and consequently the energy partition and the atmospheric water content. The second coupling option explicitly allows the water and carbon fluxes to use the same pathway through the plant canopy resistance parametrisation. Detailed evaluation will be performed in task T5.4. In addition, further improvements are also planned under task T5.3 where model parameters will be further optimized for better water, energy and CO_2 fluxes and to mitigate NWP scores' degradations.

5 Nitrogen cycle

Nitrous oxide (N_2O), nitric oxide (NO) and ammonia (NH_3) are reactive nitrogen species of global-scale relevance: N_2O is the third most important anthropogenic greenhouse gas and currently the dominant stratospheric ozone-depleting substance, while NO and NH_3 are key precursors of tropospheric ozone and secondary inorganic aerosols, with direct implications for radiative forcing, air quality, and the deposition of reactive nitrogen onto remote ecosystems. Soils are the largest natural source of these components, and their fluxes are strongly modulated by soil pH through the microbial processes of nitrification, denitrification, and NH_3 volatilization, making an accurate, pH-sensitive representation of these pathways essential for Earth system models (ESMs) to capture the coupling between the terrestrial nitrogen cycle, the global carbon sink, and the chemistry of the atmosphere.

5.1 Status of developments

This work includes into CLM the enhanced soil nitrogen cycling scheme based on Val Martin et al. (2023) approach called "hole-in-the-pipe" (Figure 8). The "hole-in-the-pipe" approach describes the soil nitrogen cycle as a unidirectional flow through a pipe, in which nitrification and denitrification act as successive segments, while lateral "holes" represent the gaseous escape of N_2O and NO, with their relative magnitude modulated by soil moisture, temperature and pH.

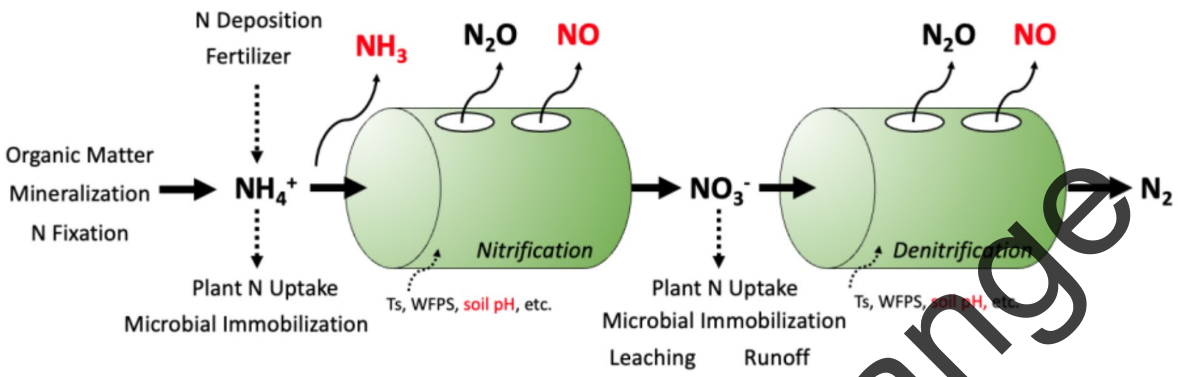

Figure 8: Schematic representation of the soil nitrogen cycling scheme implemented in CLM, adapted from Val Martin et al. (2023), following the "holes-in-the-pipe" conceptual framework. Variables highlighted in red denote the new processes and dependencies introduced in this work relative to the default CLM configuration.

The key advances are the following: (i) replacement of the constant N_2O fraction from nitrification with a soil-pH-dependent function, together with the inclusion of the N-mineralization term in the potential nitrification rate, previously missing in CLM; (ii) adoption of the modified denitrification scheme in which both gross denitrification rates and the stoichiometry of end products (N_2:N_2O ratio) are made sensitive to soil pH; (iii) introduction of a previously absent module for NO emissions as a by-product of nitrification and denitrification, including rain-pulse dynamics over previously dry soils and a canopy reduction factor (CRF) accounting for in-canopy NO uptake; (iv) implementation of NH_3 volatilisation scheme, regulated by a soil-pH response function; and (v) replacement of the global uniform CLM soil pH value (6.5) with gridded Harmonized World Soil Database data (FAO, 2012), regridded to model resolution and distributed across topsoil (0-30cm) and subsoil layers (30-100cm).

The significance of these developments lies in equipping CLM with a mechanistic representation of the sensitivity of N_2O, NO, and NH_3 emissions to soil pH

(Figure 9), a master variable governing land management practices such as liming, biochar application, and, most notably, enhanced rock weathering (ERW).

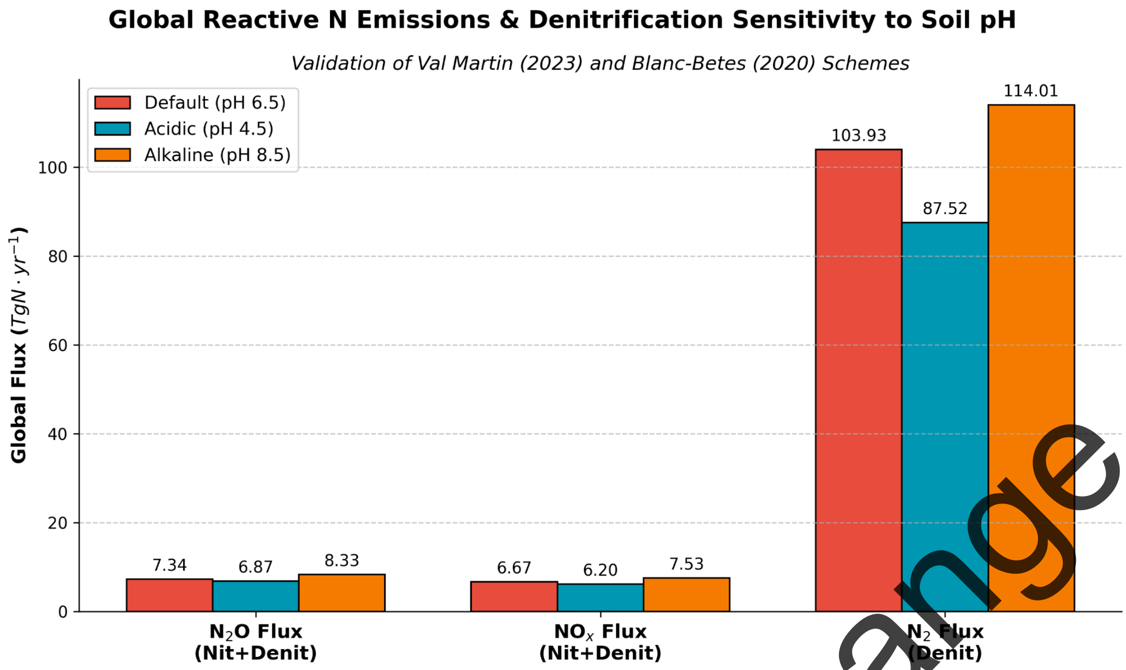

Figure 9: Sensitivity of global reactive nitrogen emissions to soil pH under three idealized global-constant pH conditions (acidic, pH 4.5; CLM-default, pH 6.5; alkaline, pH 8.5), used to validate the Val Martin et al. (2023) parameterisations. While total N_2O and NO_x fluxes show modest sensitivity to pH (~13% variation between acidic and alkaline conditions), denitrification-derived N_2 fluxes increase with pH (87.5 -> 103.9), consistent with the pH-dependent denitrification rate function. Values represent global terrestrial fluxes from nitrification and denitrification pathways.

Although these modifications act directly on the nitrogen cycle, their implications for the carbon cycle are substantial, since the tight stoichiometric coupling between carbon and nitrogen means that nitrogen availability constrains net primary productivity (NPP), carbon allocation, soil organic matter decomposition, and plant nitrogen use efficiency (NUE) (Figure 10). By more faithfully resolving gaseous nitrogen losses and the competition among nitrification, denitrification, microbial immobilization, and plant uptake, the model delivers a more coherent representation of nitrogen limitation on terrestrial carbon sequestration.

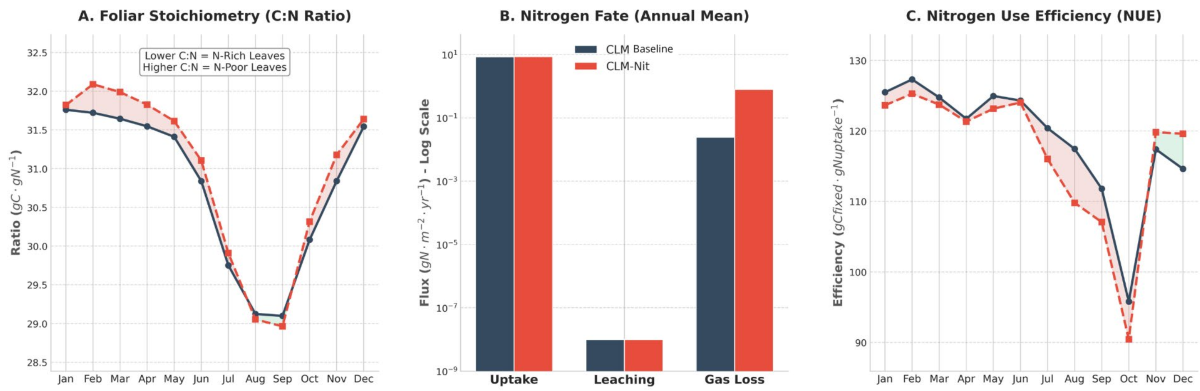

Figure 10: Plant nitrogen economy and fate in CLM with the novel nitrogen scheme (CLM-Nit, red, spatially constant pH 6.5 - default) relative to the default CLM (without nitrogen implementation, CLM Baseline, black), averaged over 2000-2015. (A) Seasonal cycle of foliar C:N ratio, indicating marginally N-poorer leaves during the active growing season under CLM-Nit. (B) Annual mean partitioning of plant N fate among uptake, leaching, and gaseous losses (log scale), showing a marked increase in gaseous losses driven by the explicit representation of NO emissions and the revised N_2O scheme. (C) Seasonal cycle of nitrogen use efficiency (NUE), showing a modest reduction in carbon fixed per unit of N taken up during the active growing season under CLM-Nit.

5.2 Future developments

A subsequent stage of this work will focus on the (v) task, which means replacing the spatially uniform soil pH value of 6.5 currently prescribed in CLM with the gridded distribution provided by the Harmonized World Soil Database (FAO, 2012), regridded to the model resolution and vertically distributed across the soil column following the topsoil (0-30 cm) and subsoil (30-100 cm) horizons. This step is a prerequisite for fully exploiting the pH-dependent parameterisations described above, as it will resolve the spatial heterogeneity of soil acidity that ultimately drives the regional variability of N_2O, NO, and NH_3 fluxes.

6 Disturbances and emissions

6.1 Status of developments

6.1.1 VOCs emissions

Terrestrial ecosystems produce a variety of BVOCs, reactive chemical species, which affect the residence time of other greenhouse gases (including methane) and are precursors of ozone and secondary organic aerosols (SOA), with important implications for ozone formation, air quality and climate. Their representation in numerical models is important in order to better assess the ecosystems responses to environmental stress conditions, as well as for understanding their impact on atmospheric chemical composition.

This section presents the improvements in the representation of BVOCs emissions parameterisations within the Model of Emissions of Gases and Aerosols from Nature (MEGAN) model (Guenther et al., 2012). MEGAN represents the emissions of several chemical compounds using both standard emission factors (EF, ϵ), representing the potential of BVOC emissions at standard conditions, and activity factors (γ), which modulate the compounds emissions in response to different environmental drivers, including sunlight, temperature, canopy density via Leaf Area Index (LAI), leaf age, drought stress, and CO_2 effect, as follows:

$$F_i = \gamma_i \sum \epsilon_{i,j} \chi_j, \quad \gamma_i = C_{CE}\, LAI\, \gamma_{light} \gamma_T \gamma_{LAI}\, \gamma_{LeafAge} \gamma_d \gamma_{CO_2}$$

The MEGAN model is assessed in two different configurations: (i) MEGAN-MOHYCAN, with the MOHYCAN canopy model (Müller et al., 2008) and (ii) MEGAN-CLM5, with the CLM5 land surface model (Lawrence et al, 2019), respectively.

In the MEGAN-MOHYCAN configuration, to account for drought stress γ_d , the "offline" parameterised drought stress (PDS) algorithm from MEGANv3 (Wang et al., 2022) was implemented, which is based on evapotranspiration (ET) data. The PDS scheme captures a two-regime drought response of isoprene emissions to f_{PET}: leaf temperature-driven stimulation (γ_{LT}) under moderate stress and substrate inhibition (γ_{sub}) under severe drought, as follows:

$$\gamma_d = \gamma_{d,max} \cdot \gamma_{sub} \cdot \gamma_{lt} \qquad \text{Eq. 1a}$$

$$\gamma_{sub} = \frac{1}{\left(1+b_1 \cdot \exp\left(a_1 \cdot (f_{pet} - 0.2)\right)\right)} \qquad \text{Eq. 1b}$$

$$\gamma_{lt} = \frac{1}{\gamma_{d,max}} + \frac{1 - \frac{1}{\gamma_{SM,max}}}{\left(1+b_2 \cdot \exp\left(a_2 \cdot (1.3 - f_{pet})\right)\right)} \qquad \text{Eq. 1c}$$

where $\gamma_{d,max}$(= 1.4) represents the maximum value of $\gamma_d \cdot \gamma_{sub}$. The parameters a_1 (= −7.45), a_2 (= −28.76), b_1 (= 3.26), and b_2 (= 2.35×10^6) control the shape of the curve (Fig. 1 in Wang et al. (2022)). The drought indicator is encapsulated in the ratio of actual ET (AET) to potential ET (PET), where AET is taken from ERA5-Land (Hersbach et al., 2020) and PET is calculated based on the Penman-Monteith equation (Allen et al., 1998) driven by ERA5 meteorological inputs (Muñoz-Sabater et al., 2021).

In the CLM5-MEGAN configuration, new parameterisations regarding both soil moisture and temperature modulation of isoprene emissions have been implemented, following Wang et al., (2022, 2024). Specifically, the new soil moisture parameterisation accounts for the drought stress using the PDS algorithm except that the ratio f_{PET} is replaced by β_{TRAN}, a mechanistically explicit indicator of drought stress computed by CLM5. Additionally, the introduced temperature parameterisation allows to better represents the stronger short- and long-term sensitivity observed for higher latitudes plant species to temperature increase during the phenological summer period.

In both the configurations, only the substrate inhibition term (γ_{sub}, Eq. 1b) is retained to avoid double counting temperature effects already numerically represented in the MOHYCAN and CLM5 models. In MEGAN-MOHYCAN, the impacts of the new parameterisations on isoprene emissions, variability and trends is assessed at local, global and regional scales, and are evaluated under two configurations: (i) a no-stress case (MEGAN, NS), where $\gamma_d = 1$, and (ii) a drought-stress case (MEGAN, DS), where $\gamma_d = \gamma_{sub}$. Within the CLM5-MODEL framework, two simulations are performed: (i) CLM5-MEGANv2, using the previous MEGAN version (v2.1; Guenther et al., 2012) and (ii) CLM5-MEGANv3, which includes the revised temperature dependence for Arctic ecosystems and the PDS algorithm (β_{TRAN}-based). Results from the MEGAN-CLM5 configuration will be evaluated against quasi-observations, which are emission estimates derived from model simulations constrained by satellite observations. Two inventories are considered, the CrIS-based (2013-2020, Li et al., 2025) and the OMI-based (2005-2017, Müller et al., 2024).

Local scale isoprene fluxes

First, a focus was put on the MOFLUX site in the central US, where isoprene flux measurements during the 2011-2012 summer droughts enable direct comparison with MEGAN-MOHYCAN simulations (Potosnak et al., 2014; Seco et al., 2015). The model is driven by local environmental conditions following Opacka et al. (2022), with gaps in meteorological data filled in using ERA5 fields. Here, we focus on the impact of the offline PDS relying on f_{PET} as a drought indicator.

In 2011, a mild drought year, modelled and observed fluxes strongly correlated (0.92) with γ_d inducing only a slight emission reduction, mainly in late July. In contrast, during the severe 2012 drought, the simulation without drought stress shows a strong positive bias from late June to October, with July–August isoprene fluxes (~12 mg $m^{-2}h^{-1}$) about twice as high as the observed values (6.14 mg $m^{-2}h^{-1}$). The inclusion of drought stress improves performance, increasing the correlation from 0.76 to 0.85, and halving the RMSE. Inhibition starts in late May and peaks in July ($f_{PET} \simeq 0.3$) in the driest conditions.

However, we noted that ERA5-Land AET shows a persistent positive bias (~1 mm day^{-1} after mid-June) relative to in situ data (Wood and Gu, 2016), likely leading to underestimated drought stress and residual overestimation of isoprene fluxes in summer 2012 (Figure 11).

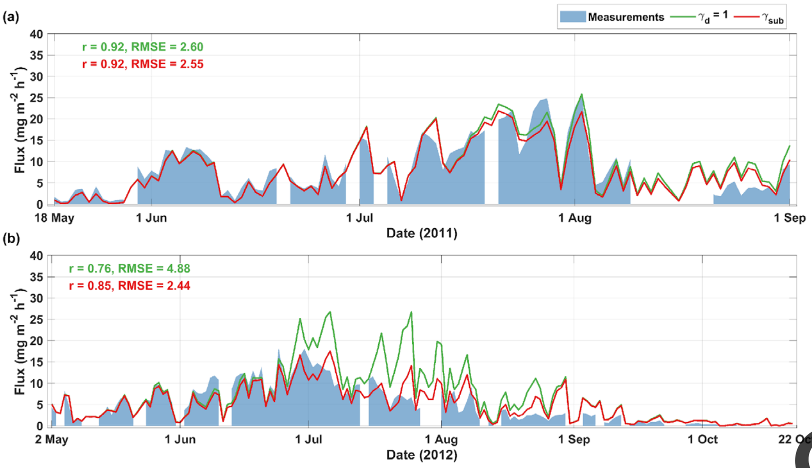

Figure 11: Daily isoprene emission fluxes (mg m^{-2} h^{-1}) at the MOFLUX site, averaged over 7-17h (CST), for (a) 2011 and (b) 2012. Isoprene observations (blue shading) are derived from field campaigns conducted in 2011 by Potosnak et al. (2014) and in 2012 by Seco et al. (2015). MEGAN-MOHYCAN simulations are shown with γ_d = 1 (in green) and with the drought stress factor $\gamma_d = \gamma_{sub}$ (in red). The Pearson correlation coefficient (r) and root-mean-square error (RMSE) are provided inset for each simulation.

Regional and global isoprene fluxes

In the CLM5-MEGAN configuration, the new drought and temperature model modifications reduce the biases of global estimates to the quasi-observational datasets used as references (Müller et al., 2024, Li et al., 2025, Table 2), decreasing global BVOC emissions by 21% over the period 2013-2017.

Table 2: Global isoprene emissions for the period 2013-2017.

Reference	Global Emissions
Li et al., 2025	448 Tg
Müller et al., 2024	395 Tg
CLM5-MEGAN3	433 Tg
CLM5-MEGAN2	546 Tg
MOHYCAN-MEGAN3	330 Tg
MOHYCAN -MEGAN2	456 Tg

Despite the improvements in global estimates, several biases persist, indicating a regional- or PFT-specific biased BVOC emissions overestimation in the tropical regions, and a slight underestimation in semi-arid biomes as well as in the mid to high-latitudes. A comparison of the monthly climatology of our simulation estimates accounting for the isoprene emissions distribution at the PFT level (considering an ESACCI dominant PFT map) confirms the persistence of a strong bias (Figure 12).

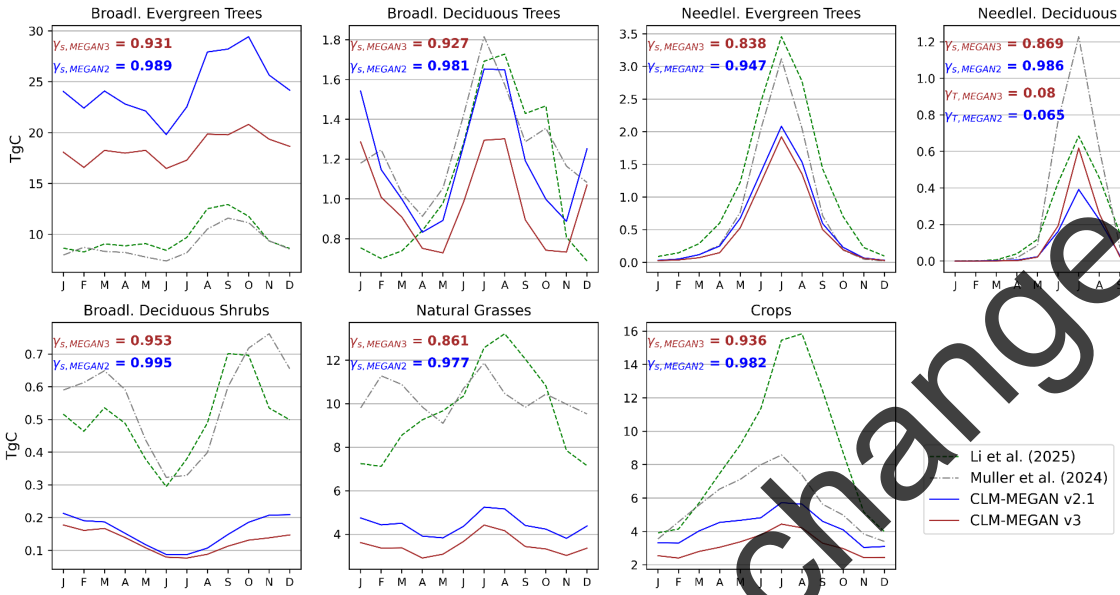

Figure 12: Monthly climatology of isoprene emissions from CLM5-MEGAN simulations vs quasi observations. Mean soil-moisture and temperature activity factors (only for needleleaf deciduous trees) are also reported inset.

Factorial simulations were performed to test the dominant contribution of environmental activity factors and therefore elucidate potential areas of improvement in future model parameterisations of BVOC emissions. In doing so, six simulations were performed, each one activating uniquely one activity factor at a time. The main environmental factors contributing to isoprene emissions were identified for every dominant plant functional types from ESA CCI (Li et al., 2018). We found sunlight (yellow) to be the most widespread isoprene emissions contributor, especially for tropical evergreen forests where water is not a limiting factor for vegetation (Figure 13). On the other hand, LAI (green) assumes relevance in low-LAI/semi-arid regions with prevailing natural grasses and shrubland ecosystems, dominated by strong seasonal vegetation variability, while temperature (red) dominates isoprene emissions in temperate and boreal regions.

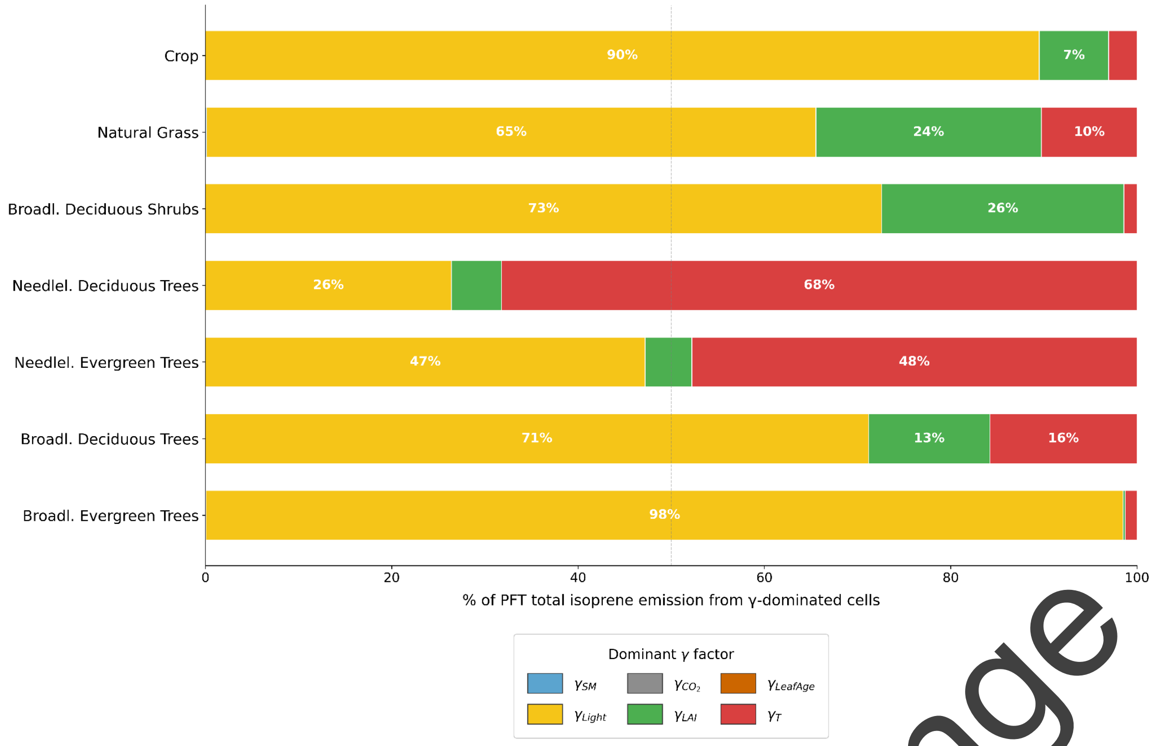

Figure 13: Drivers of isoprene variability, averaged for the ESACCI PFT considered in CLM5-MEGAN3 factorial simulations.

In the MEGAN-MOHYCAN configuration, drought stress reduces isoprene emissions by about 30%, from 456 to 330 Tg (Table 2), and mitigates their positive trend from 0.8 to 0.4%yr-1 over 2005-2024, reflecting increasing drought intensity. This reduction in trends is widespread, with particularly strong effects in Africa. Overall, drought dampens both the magnitude and the variability of emissions, while also modifying seasonal cycles, with impacts varying strongly across regions (Figure 14). The strongest emission reductions occur in water-limited and seasonally dry environments. Among the regions considered, the relatively low-emitting western US exhibits the largest decrease (~70%), followed by declines of ~40-50% across northern Australia, southern Europe, northern and southern Africa, India, and northeast Brazil, and about 30% in Mexico. In contrast, impacts remain weaker in high-emission, moisture-rich regions such as the Amazon Basin (-13%), southeastern US and central Africa (−10%) and are minimal in southeast China (-3%). Besides magnitude, drought substantially alters emissions' seasonality. In several regions, emissions are suppressed during the warmest and driest months, dampening or shifting seasonal peaks. Drought suppresses the spring maximum of bimodal cycles in Mexico, Northern Africa and India, shifting the emission peaks in the second part of the year.

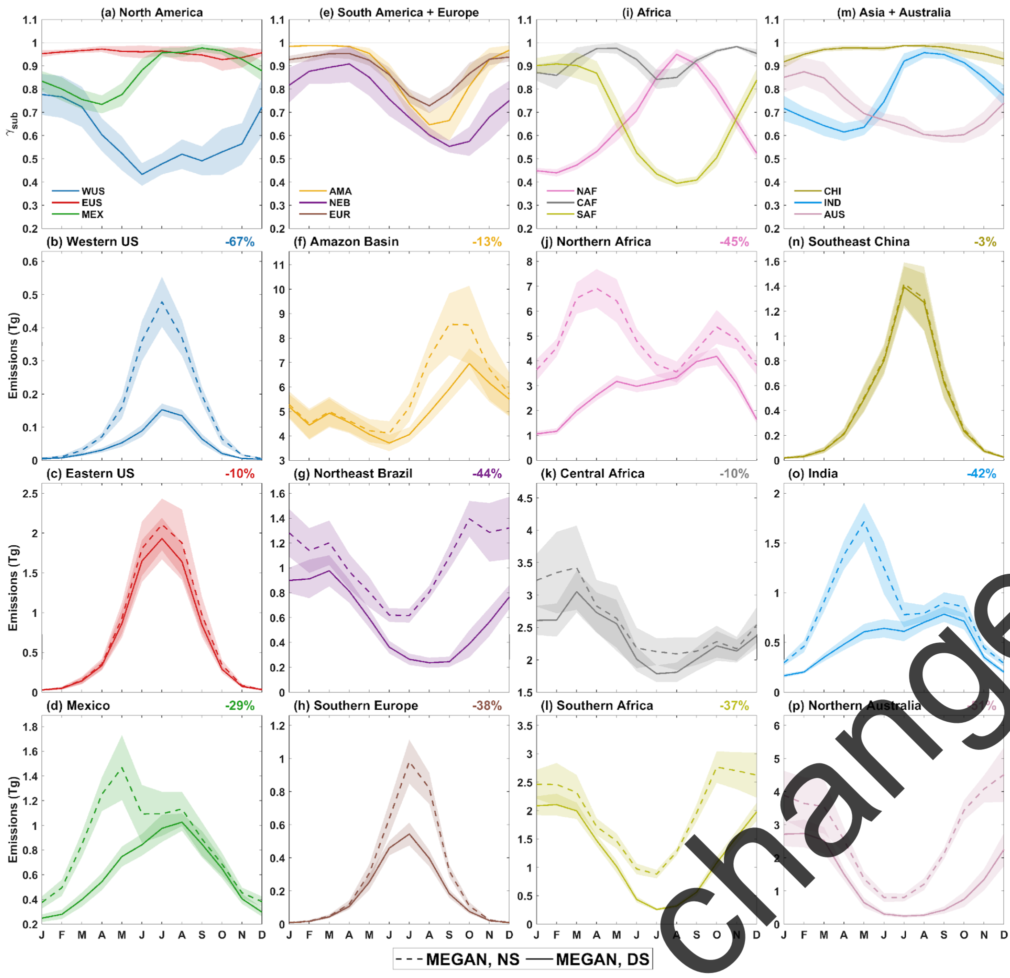

Figure 14: Seasonal variability of the 2005-2024 mean drought stress factor (γ_{sub}, top row) and isoprene emissions with standard deviations. Emissions are estimated with MEGAN-MOHYCAN without drought (MEGAN,NS; dashed) and with drought inhibition (MEGAN,DS; solid). The inset shows the % reduction in annual emissions relative to NS. Regions: WUS (Western US), EUS (Eastern US), MEX (Mexico), AMA (Amazon Basin), NEB (Northeast Brazil), EUR (Southern Europe), NAF (Northern Africa), CAF (Central Africa), SAF (Southern Africa), CHI (Southeast China), IND (India), AUS (Northern Australia).

6.1.2 Fire modules

Accurate predictions of burnt area in ESM are essential to better estimate carbon emissions and assess potential future climate–fire feedback (Rabin et al., 2017). However, current fire modules within land surface models are still unable to adequately capture interannual variations in burnt area (Hantson et al., 2020; Li et al., 2024). Empirical models suggest that this limitation may partly arise from an insufficient representation of fuel build-up conditions (Forkel et al., 2019; Haas et al., 2024; Kuhn-Régnier et al., 2021).

To address this issue, we focus on the Li model (Li et al., 2012) implemented in CLM5, since together with SPITFIRE it is one of the fire schemes most widely used in CMIP6 simulations (Li et al., 2024). Forest fires in the Li scheme (excluding deforestation fires) are represented by a total number of ignitions per mean fire area:

$$A_b = N_f \, a$$

where N_f represents the final number of ignitions and *a* the mean fire spread area. At the same time N_f is represented by:

$$N_f = N_i \, f_b \, f_m \, f_{se,o}$$

Where f_b and f_m are fractions (0-1) representing fuel availability and combustibility, respectively, while $f_{se,o}$ denotes the fraction of fires not suppressed by humans.

Specifically, f_b is based on total carbon biomass (i.e. carbon allocated to leaves, stems, litter and woody debris), however, fine fuels are generally more relevant for ignition success than total biomass, because their high surface-area-to-volume ratio allows them to dry rapidly and ignite more easily than coarse fuels (Rothermel, 1972). Thus, aiming to better capture burnt area variability across years due to wet-dry processes, we ran several experiments modifying how fuel availability for burning is represented, shifting the current focus from total biomass to fine fuel accumulation (we focus on litter, and leaf carbon content from grassy PFTs only). We also tested different scaling relationships between fuel availability and fire occurrence, ranging from linear to exponential. Here, we examine the results of a single experiment across multiple biomes.

Results show that focusing on live and dead fine fuels increases the variability of f_b across years (Figure 15). In addition, it changes the seasonal peak of fuel available to burn in most biomes, mainly due to the opposite seasonal patterns of live and dead biomass (data not shown).

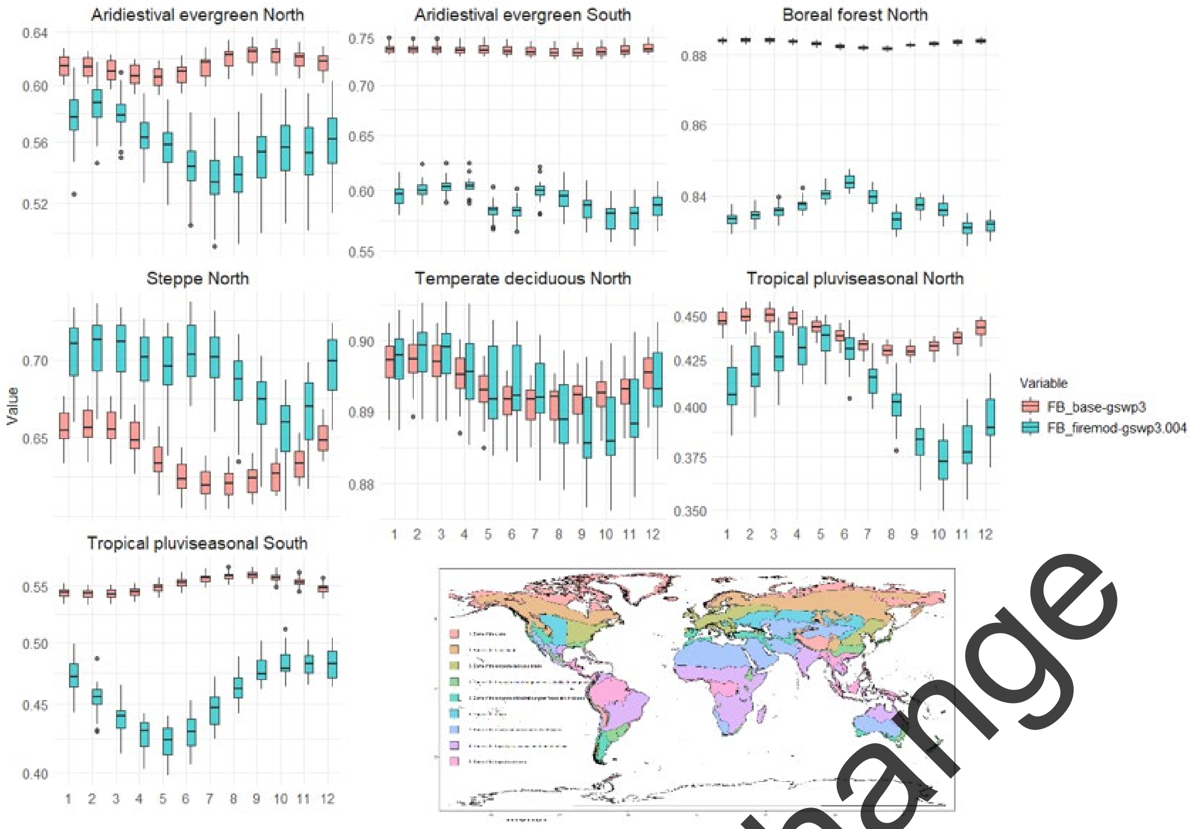

Figure 15: Interannual variability of the fuel availability factor across months. Red boxplots represent the original model, whereas blue boxplots represent the modified version focused on fine fuels.

However, despite increasing the sensitivity to interannual variations in fuel availability, this is not clearly reflected in burnt area variability, with similar years still showing the largest peaks. This highlights that burnt areas in the model are primarily driven by other factors (such as weather conditions) rather than fuel availability alone (Figure 16).

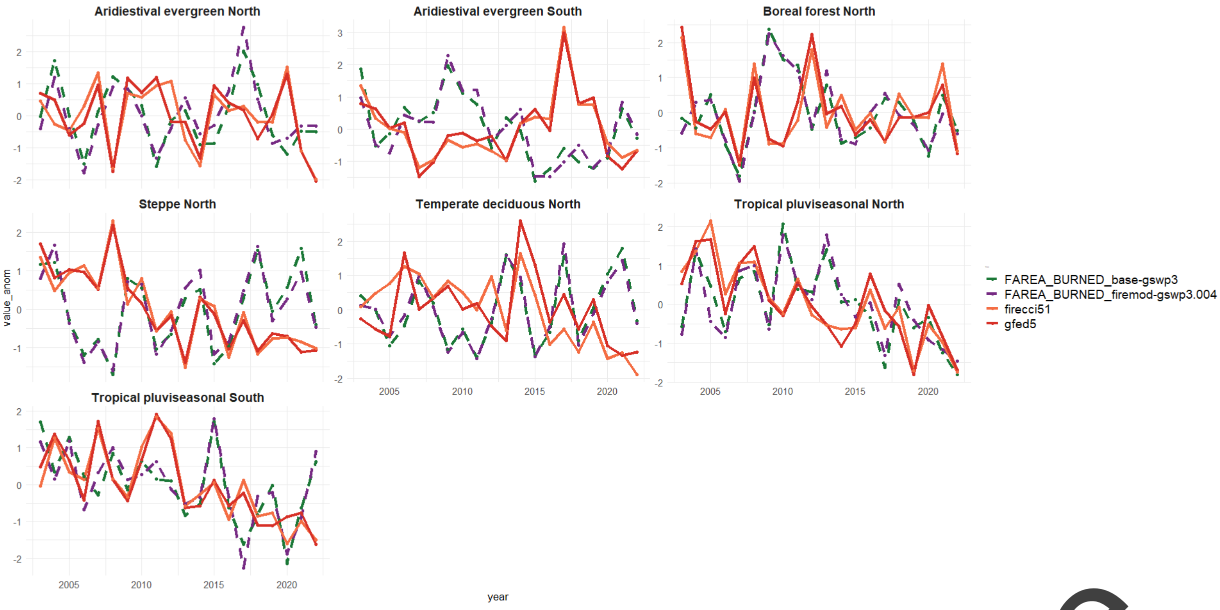

Figure 16: Standardized anomalies of burned area for the base model (FAREA_BURNED_base-gswp3, green dashed), modified model (FAREA_BURNED_firemod-gswp3.004, purple dashed), and observational datasets (firecci5.1 and gfed5, orange and red solid lines) across selected biomes over the period 2001–2022. Anomalies are calculated relative to the long-term mean of each dataset.

Thus, we also explore the role of fuel combustibility (f_m) on burnt area variability, which is based on relative humidity (a weighted average of daily values and 30-day running mean) and soil moisture:

$$f_m = f_{RH} f_\beta$$

Since we observed a delayed response of the fire season in the original model (see Figure 17), we performed several sensitivity experiments targeting potential limitations in the representation of physical processes linked to fuel moisture. First, we removed the soil moisture effect, as dead fine fuels are weakly dependent on soil moisture conditions and soil moisture is expected to have a delayed response. Second, we removed the long-term precipitation effect, since dead fine fuels are also not strongly conditioned by antecedent precipitation.

Figure 17: Seasonal cycle of standardized fire combustibility anomalies, comparing the base model (FIRE_M_base-gswp3), two modified model configurations removing soil moisture and long-term precipitation effects (dashed lines), and observed fire activity (firecci.51 and gfed5, orange and red solid lines).

However, sensitivity experiments only produce moderate changes in the seasonal cycle of fuel combustibility, with noticeable differences restricted to a few biomes (Figure 17). Moreover, the simulated combustibility seasonality does not consistently match the observed burnt area dynamics, suggesting a mismatch between the timing of modelled drivers and observed fire activity.

Looking at the combined effect, results suggest a slight improvement in the representation of wet-dry processes affecting burned area (Figure 18). The modified model shows a better alignment between burned area and the fuel availability — combustibility space, with high burned area years (large red points) concentrating in the high fuel — high combustibility quadrant and low burned area years in the opposite corner, indicating increased model sensitivity to wet-dry driven fire processes. However, the improvement remains modest and further model development is needed to fully capture the role of fuel accumulation and moisture dynamics across different biomes (see next section).

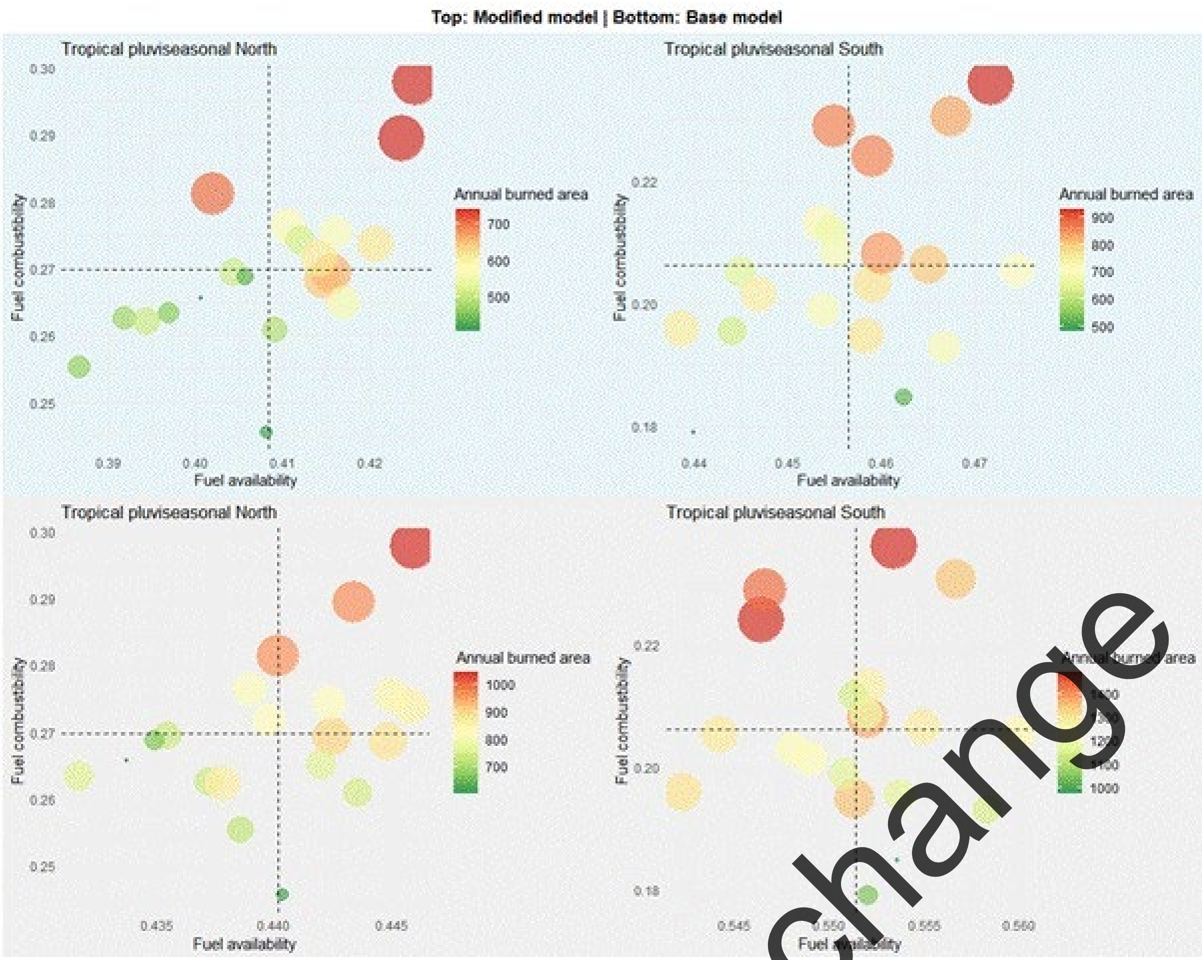

Figure 18: Annual burned area (point size and color) across the fuel availability- combustibility space for the modified model (top, blue background) and base model (bottom, grey background) across two tropical pluviseasonal biomes. Points represent individual years. Dashed lines indicate biome means. Red points indicate years with higher burned area.

6.2 Future developments

6.2.1 BVOCs emissions

Within the MOHYCAN-MEGAN coupled model, given the substantial impact of the parameterised drought stress (PDS) parameterisation, a comprehensive global and regional evaluation will be conducted as part of the WP4, using satellite-derived isoprene columns and simulations with the MAGRITTEv1.2 in-house chemistry-transport model.

Within the CLM5-MEGAN coupled model, additional improvements in the parameterisations will be conducted based on new observational studies. Further analysis will focus on the impacts of compound hot-dry extreme events on BVOC emissions, particularly on their effects on the drivers' dominance.

6.2.2 Fire module

Several improvements are planned to further enhance the model's representation of fire dynamics. First, fine-tuning the parameterisation linking fuel availability to interannual burned area variability remains a priority, as year-to-year variation in the current version remains poorly represented. Second, fire combustibility will be reformulated using vapour pressure deficit (VPD) as the primary driver, replacing relative humidity, given that VPD more accurately reflects atmospheric moisture demand and is increasingly recognized as a key predictor of fire activity (Clarke et al., 2022). Additionally, fuel combustibility will be linked to fire spread area as a proxy for landscape fragmentation, addressing a limitation already identified in previous studies (Haas et al., 2024). Finally, post-fire emission estimates will be improved by implementing recently updated emission factors (Shahid et al., 2024) and transitioning from fixed to moisture-dependent combustion completeness factors, which is expected to better represent observed emissions across fire regimes. Results will be compared against an empirical model following IPCC guidelines developed at CMCC (Aquino et al., 2026) following the methodology adopted in the Italian National Reporting of GHG emissions from forest fires.

7 References

Allen, R.G., Pereira, L.S., Raes, D. and Smith, M., 1998. 'Crop evapotranspiration: Guidelines for computing crop water requirements', Food and Agriculture Organization of the United Nations (FAO), Irrigation and Drainage Paper No. 56, Rome.

Aquino, C., Bacciu, V., Chiriacò, M.V. et al., 2026. 'An Earth Observation-based Tier 3 framework for monitoring greenhouse gas emissions from forest fires in Italy' *Sci Rep*. https://doi.org/10.1038/s41598-026-55318-x

Boussetta, S., Balsamo, G., Arduini, G., Choulga, M., Albergel, C., Beljaars, A., Wedi, N., Lawrence, H., de Rosnay, P., Muñoz-Sabater, J. and Agustí-Panareda, A., 2021. 'ECLand: The ECMWF Land Surface Modelling System', *Atmosphere*, 12(6), p.723. https://doi.org/10.3390/atmos12060723

Clarke, H., Nolan, R.H., De Dios, V.R., Bradstock, R., Griebel, A., Khanal, S. and Boer, M.M., 2022. 'Forest fire threatens global carbon sinks and population centres under rising atmospheric water demand', *Nature Communications*, 13(1). https://doi.org/10.1038/s41467-022-34966-3

Cotrim da Cunha, L., Buitenhuis, E.T., Le Quéré, C., Giraud, X. and Ludwig, W., 2007. 'Potential impact of changes in river nutrient supply on global ocean biogeochemistry', *Global Biogeochemical Cycles*, 21, GB4007. https://doi.org/10.1029/2006GB002718

FAO/IIASA/ISRIC/ISS-CAS/JRC, 2012. 'Harmonized World Soil Database (Version 1.2)', FAO, Rome and IIASA, Laxenburg.

Farquhar, G. D., von Caemmerer, S. and Berry, J. A. (1980). A biochemical model of photosynthetic CO2 assimilation in leaves of c3 species. Planta, 149(1), 78–90, doi:10.1007/BF00386231.

Forkel, M., Andela, N., Harrison, S.P., Lasslop, G., Van Marle, M., Chuvieco, E., Dorigo, W., Forrest, M., Hantson, S., Heil, A., Li, F., Melton, J., Sitch, S., Yue, C. and Arneth, A., 2019. 'Emergent relationships with respect to burned area in global satellite observations and fire-enabled vegetation models', *Biogeosciences*, 16(1), pp.57–76. https://doi.org/10.5194/bg-16-57-2019

Geer, A.J., 2016. 'Significance of changes in medium-range forecast scores', *Tellus A: Dynamic Meteorology and Oceanography*, 68, 30229. https://doi.org/10.3402/tellusa.v68.30229

Guenther, A.B., Jiang, X., Heald, C.L., Sakulyanontvittaya, T., Duhl, T., Emmons, L.K. and Wang, X., 2012. 'The Model of Emissions of Gases and Aerosols from Nature version

2.1 (MEGAN2.1): an extended and updated framework for modeling biogenic emissions', *Geoscientific Model Development*, 5, pp.1471–1492. https://doi.org/10.5194/gmd-5-1471-2012

Haas, O., Keeping, T., Gomez-Dans, J., Prentice, I.C. and Harrison, S.P., 2024. 'The global drivers of wildfire', *Frontiers in Environmental Science*, 12, 1438262. https://doi.org/10.3389/fenvs.2024.1438262

Hantson, S., Kelley, D.I., Arneth, A., Harrison, S.P., Archibald, S., Bachelet, D., Forrest, M., Hickler, T., Lasslop, G., Li, F., Mangeon, S., Melton, J.R., Nieradzik, L., Rabin, S.S., Prentice, I.C., Sheehan, T., Sitch, S., Teckentrup, L., Voulgarakis, A. and Yue, C., 2020. 'Quantitative assessment of fire and vegetation properties in historical simulations with fire-enabled vegetation models from the Fire Model Intercomparison Project', *Geoscientific Model Development*, 13, pp.3299–3318. https://doi.org/10.5194/gmd-13-3299-2020

Hersbach, H., Bell, B., Berrisford, P., Hirahara, S., Horányi, A., Muñoz-Sabater, J., et al., 2020. 'The ERA5 global reanalysis', *Quarterly Journal of the Royal Meteorological Society*, 146(730), pp.1999–2049. https://doi.org/10.1002/qj.3803

Jarvis, P. J. (1976). The interpretation of the variations in leaf-water potential and stomatal conductance found in canopies in the field. Phil. Trans. R. Soc. London, B723, 385–610.

Kuhn-Régnier, A., Voulgarakis, A., Nowack, P., Forkel, M., Prentice, I.C. and Harrison, S.P., 2021. 'The importance of antecedent vegetation and drought conditions as global drivers of burnt area', *Biogeosciences*, 18(12), pp.3861–3879. https://doi.org/10.5194/bg-18-3861-2021

Lawrence, D.M., Fisher, R.A., Koven, C.D., Oleson, K.W., Swenson, S.C., Bonan, G., et al., 2019. 'The Community Land Model version 5: Description of new features, benchmarking, and impact of forcing uncertainty', *Journal of Advances in Modeling Earth Systems*, 11, pp.4245–4287. https://doi.org/10.1029/2018MS001583

Li, F., Zeng, X.D. and Levis, S., 2012. 'A process-based fire parameterization of intermediate complexity in a dynamic global vegetation model', *Biogeosciences*, 9(7), pp.2761–2780.
https://doi.org/10.5194/bg-9-2761-2012

Li, W., MacBean, N., Ciais, P., Defourny, P., Lamarche, C., Bon- temps, S., Houghton, R. A., and Peng, S., 2018. 'Gross and net land cover changes in the main plant functional types derived from the annual ESA CCI land cover maps (1992–2015)', *Earth Syst. Sci. Data*, 10, 219–234. https://doi.org/10.5194/essd-10-219-2018

Li, F., Song, X., Harrison, S.P., Marlon, J., Lin, Z., Leung, L.R., Schwinger, J., Marécal, V., Wang, S., Ward, D., Dong, X., Lee, H., Nieradzik, L., Rabin, S.S. and Séférian, R., 2024. 'Evaluation of global fire simulations in CMIP6 Earth system models', *Geoscientific Model Development*, 17(23), pp.8751–8771. https://doi.org/10.5194/gmd-17-8751-2024

Li, H., Ciais, P., Kumar, P., Hauglustaine, D.A., Chevallier, F., Broquet, G., et al., 2025. 'Global biogenic isoprene emissions 2013–2020 inferred from satellite isoprene observations', *Earth System Science Data*, 17(12), pp.7035–7054.

Müller, J.-F., Stavrakou, T., Wallens, S., De Smedt, I., Van Roozendael, M., Potosnak, M.J., Rinne, J., Munger, B., Goldstein, A. and Guenther, A.B., 2008. 'Global isoprene emissions estimated using MEGAN, ECMWF analyses and a detailed canopy environment model', *Atmospheric Chemistry and Physics*, 8, pp.1329–1341. https://doi.org/10.5194/acp-8-1329-2008

Müller, J.-F., Stavrakou, T., Oomen, G.M., Opacka, B., De Smedt, I., Guenther, A., et al., 2024. 'Bias correction of OMI HCHO columns based on FTIR and aircraft measurements and impact on top-down emission estimates', *Atmospheric Chemistry and Physics*, 24(4), pp.2207–2237.

Muñoz-Sabater, J., Dutra, E., Agustí-Panareda, A., Albergel, C., Arduini, G., Balsamo, G., Boussetta, S., Choulga, M., Harrigan, S., Hersbach, H., Martens, B., Miralles, D.G., Piles, M., Rodríguez-Fernández, N.J., Zsoter, E., Buontempo, C. and Thépaut, J.-N., 2021. 'ERA5-Land: a state-of-the-art global reanalysis dataset for land applications', *Earth System Science Data*, 13, pp.4349–4383. https://doi.org/10.5194/essd-13-4349-2021

Opacka, B., Müller, J.-F., Stavrakou, T., Miralles, D.G., Koppa, A., Pagán, B.R., et al., 2022. 'Impact of drought on isoprene fluxes assessed using field data, satellite-based GLEAM soil moisture and HCHO observations from OMI', *Remote Sensing*, 14(9), 2021. https://doi.org/10.3390/rs14092021

Potosnak, M.J., LeStourgeon, L., Pallardy, S.G., Hosman, K.P., Gu, L., Karl, T., et al., 2014. 'Observed and modeled ecosystem isoprene fluxes from an oak-dominated temperate forest and the influence of drought stress', *Atmospheric Environment*, 84, pp.314–322. https://doi.org/10.1016/j.atmosenv.2013.11.055

Rabin, S.S., Melton, J.R., Lasslop, G., Bachelet, D., Forrest, M., Hantson, S., Kaplan, J.O., Li, F., Mangeon, S., Ward, D.S., Yue, C., Arora, V.K., Hickler, T., Kloster, S., Knorr, W., Nieradzik, L., Spessa, A., Folberth, G.A., Sheehan, T., Voulgarakis, A., Kelley, D.I., Prentice, I.C., Sitch, S., Harrison, S.P. and Arneth, A., 2017. 'The Fire Modeling Intercomparison Project (FireMIP), phase 1: Experimental and analytical protocols with detailed model descriptions', *Geoscientific Model Development*, 10(3), pp.1175–1197. https://doi.org/10.5194/gmd-10-1175-2017

Rothermel, R.C., 1972. 'A Mathematical Model for Predicting Fire Spread', United States Department of Agriculture, Forest Service Research Paper INT-115.

Seco, R., Karl, T., Guenther, A., Hosman, K.P., Pallardy, S.G., Gu, L., et al., 2015. 'Ecosystem-scale volatile organic compound fluxes during an extreme drought in a broadleaf temperate forest of the Missouri Ozarks (central USA)', *Global Change Biology*, 21(10), pp.3657–3674. https://doi.org/10.1111/gcb.12980

Shahid, S.B., Lacey, F.G., Wiedinmyer, C., Yokelson, R.J. and Barsanti, K.C., 2024. 'NEIVAv1.0: Next-generation Emissions InVentory expansion of Akagi et al. (2011) version 1.0', *Geoscientific Model Development*, 17(21), pp.7679–7711. https://doi.org/10.5194/gmd-17-7679-2024

Smith, S.V. and Hollibaugh, J.T., 1993. 'Coastal metabolism and the oceanic organic carbon balance', *Reviews of Geophysics*, 31(1), pp.75–89. https://doi.org/10.1029/92RG02584

Val Martin, M., Blanc-Betes, E., Fung, K.M., Kantzas, E.P., Kantola, I.B., Chiaravalloti, I., et al., 2023. 'Improving nitrogen cycling in a land surface model (CLM5) to quantify soil N_2O, NO, and NH_3 emissions from enhanced rock weathering with croplands', *Geoscientific Model Development*, 16(20), pp.5783–5801. https://doi.org/10.5194/gmd-16-5783-2023

Wang, H., Lu, X., Seco, R., Stavrakou, T., Karl, T., Jiang, X., et al., 2022. 'Modeling isoprene emission response to drought and heatwaves within MEGAN using evapotranspiration data and by coupling with the Community Land Model', *Journal of Advances in Modeling Earth Systems*, 14, e2022MS003174. https://doi.org/10.1029/2022MS003174

Wang, H., Welch, A.M., Nagalingam, S., et al., 2024. 'High temperature sensitivity of Arctic isoprene emissions explained by sedges', *Nature Communications*, 15, 6144. https://doi.org/10.1038/s41467-024-49960-0

Wood, J. and Gu, L., 2016. 'AmeriFlux US-MOz Missouri Ozark site', Oak Ridge National Laboratory and University of Missouri.